Nonisothermal kinetic analysis of decomposition of CuCO3.Cu(OH)2 and 2ZnCO3.3Zn(OH)2

Prithviraj Gupta**, Rohit Kumar Singh***, Akshay Patil*** and Anup Kumar Sadhukhan*

*, *** *Chemical Engineering Department, National Institute of Technology Durgapur 713209, India*

** *Metallurgical and Material Engineering Department, Jadavpur University, Kolkata 700032, India*

* *Corresponding Author: anupkumar.sadhukhan@che.nitdgp.ac.in*

Submitted : 03-10-2021

Revised : 21-11-2021

Accepted : 20-12-2021

ABSTRACT

Thermal decomposition of copper (II) carbonate hydroxide (CCH), $CuCO_3.Cu(OH)_2$ and zinc hydroxide carbonate (ZHC), $2ZnCO_3.3Zn(OH)_2$ is widely used for the synthesis of copper and zinc oxides. Kinetic modelling, identification of the rate-controlling step and change in thermodynamic properties of these decomposition reactions have not been reported adequately in the literature. In the present work, the kinetic behaviour of nonisothermal thermal decomposition of $CuCO_3.Cu(OH)_2$, and $2ZnCO_3.3Zn(OH)_2$ has been investigated using thermogravimetric (TG) analysis, employing model-free iso-conversional as well as model-fitting methods. Mean apparent activation energy (E_a) values, estimated by various iso-conversional methods (KAS, Starink, FWO, Kissinger and Vyazovkin), were found to be in close agreement (104.9-111.2 kJ.mol^{-1} for $CuCO_3.Cu(OH)_2$ and 192.8-197.9 kJ.mol^{-1} for $2ZnCO_3.3Zn(OH)_2$). E_a decreased significantly with an increase in conversion for $CuCO_3.Cu(OH)_2$, while it increased, peaked and then decreased with conversion for $2ZnCO_3.3Zn(OH)_2$. It indicates that both decomposition reactions are not single-step. Avrami-Erofeev model of order 2.5 was found to explain the experimental TG data well for $CuCO_3.Cu(OH)_2$ decomposition, while $2ZnCO_3.3Zn(OH)_2$ decomposition followed the chemical reaction model of order 1.75. Positive changes in the thermodynamic properties, enthalpy and Gibbs free energy for both samples showed that these endothermic decomposition reactions were not spontaneous. The difference between E_a and ΔH was found to be low; 3.9-4.5 kJ.mol^{-1}and 4.0-4.6 kJ.mol^{-1} for $CuCO_3.Cu(OH)_2$ and $2ZnCO_3.3Zn(OH)_2$ respectively, indicating the reactions to be favourable. The thermodynamic properties, though not influenced by the iso-conversional method and the rate of heating, varied significantly with the conversion. FTIR analysis of the gases evolved from decomposition showed that dehydration started before the initiation of decarboxylation, followed by simultaneous progress of both these reactions for $CuCO_3.Cu(OH)_2$ and $2ZnCO_3.3Zn(OH)_2$.

Keywords: Thermogravimetric Analysis; Iso-Conversional Method; Activation Energy; Kinetic Models

INTRODUCTION

Malachite, $CuCO_3.Cu(OH)_2$ is a commonly occurring monoclinic copper (II) carbonate hydroxide (CCH) (basic copper carbonate) mineral (Frost *et al.*, 2002). Its thermal decomposition is widely employed in the synthesis of nano-scale copper and copper oxides, particularly for the manufacture of catalysts (Uzunov and Klissurski *et al.*, 1984).

Zinc oxide (ZnO), which has diverse applications in electronic components, gas sensitisation and catalysts (Kanari *et al.*, 2004; Liu *et al.*, 2004), is often synthesised by decomposition of zinc hydroxide carbonate (ZHC), $2ZnCO_3.3Zn(OH)_2$ precursors. These are energetically more favourable than other precursors like hydroxides, carbonates, etc., due to the lower thermal decomposition temperature (Kanari *et al.*, 2004; Liu *et al.*, 2004).

Malachite, when heated, loses H_2O and CO_2, forming CuO (Brown *et al.*, 1984).

$$CuCO_3.Cu(OH)_2 \rightarrow 2CuO + H_2O + CO_2 \quad (1)$$

Brown *et al*. (1984), using TGA-EGA, proposed that the decomposition of malachite in Helium followed single-step decomposition at 380 ^oC with simultaneous evolution of CO_2 and water. Henmi *et al*. (1986) also showed that the decomposition of malachite in CO_2 and N_2 atmospheres at high pressure took place rapidly in one step with no intermediates formed. Pourmortazavi *et al*. (2009) observed that the micro-particles of CCH decomposed in the temperature range of 230-330 ^oC while the decomposition for nanoparticles took place within 245-315 ^oC in a single-step.

A limited number of thermogravimetric analyses of thermal decomposition of ZHC have been reported in the literature.

$$2ZnCO_3.3Zn(OH)_2 = 5ZnO + 3H_2O + 2CO_2 \quad (2)$$

Henmi *et al*. (1986) observed simultaneous evolution of water and CO_2 for thermal decomposition of hydrozincite, $2ZnCO_3.3Zn(OH)_2$. Liu *et al*. (2004) also reported a single-stage ZHC decomposition in a nitrogen atmosphere.

Theory of kinetic analysis

Fractional conversion of a solid reactant (α) when it is subjected to thermogravimetric analysis, is defined as (Jankovic, 2008):

$$\alpha = \frac{m_0 - m_t}{m_0 - m_\infty} \quad (3)$$

m_0, m_t and m_∞ are the initial, instantaneous and residual fully converted dry sample mass respectively.

Equation (4) represents the kinetic rate equation after incorporating the Arrhenius equation with $f(\alpha)$ as the reaction mechanism model, A the pre-exponential factor, E_a the apparent activation energy and T the sample temperature.

$$\frac{d\alpha}{dt} = k(T).f(\alpha) = A.exp\left(-\frac{E_a}{RT}\right).f(\alpha) \quad (4)$$

For a constant heating rate, β, $\frac{dT}{dt} = \beta$ (5)

Combining Equations (4) and (5) $\frac{d\alpha}{dT} = \frac{A}{\beta}.exp\left(-\frac{E_a}{RT}\right).f(\alpha)$ (6)

Integral of the inverse of $f(\alpha)$ is expressed as:

$$g(\alpha) = \int_0^\alpha \frac{d\alpha}{f(\alpha)} = \frac{A}{\beta}.\int_{T_0}^{T}(exp\left(-\frac{E_a}{RT}\right).dT = \frac{A}{\beta}\int_0^T(exp\left(-\frac{E_a}{RT}\right).dT \quad \text{(as } T_0 \text{ is small)} \quad (7)$$

Substituting $x = \frac{E_a}{RT}$

(8)

$$g(\alpha) = \frac{AE_a}{\beta R}.p(x) = k(T).t \quad (9)$$

where $p(x) = \int_x^\infty \frac{\exp(-x)}{x^2}.dx$ (10)

p(x), having no analytical solution, may be estimated using one of the following empirical approximating function.

(1) Doyle approximation: $p(x) = exp(-1.0518x - 5.33)$ (11)

(2) Coats-Redfern approximation: $p(x) = \frac{\exp(-x)}{x^2}.[1 - \frac{2}{x}]$ (12)

(3) Senum and Yang: $p(x) = \frac{\exp(-x)}{x}.\frac{x^3+18x^2+86x+96}{x^4+20x^3+120x^2+240x+120}$ (13)

$g(\alpha)$ is evaluated using different kinetic models (Khawam and Flanagan, 2006; Kurt and Koca, 2016, Gupta *et al*., 2017).

Model fitting methods

Coats-Redfern (CR) *method*: Using CR approximation (Equation 12) for the temperature integration, Equation (9) for first-order reactions is expressed as: $\ln\left[\frac{g(\alpha)}{T^2}\right] = \ln\left[\frac{AR}{\beta E_a}.(1 - \frac{2RT}{E_a})\right] - \frac{E_a}{RT}$ (14)

However, such model-fitting methods have been criticised as a regression method may lead to indistinguishable fits and do not ensure a clear separation between *k(T)* and *f(α)* (Vyazovkin, 1999).

Model-free (iso-conversional) methods

In a reaction involving a solid phase with a complex reaction mechanism, the kinetic parameters are often found to vary with the conversion, which may be captured well by model-free iso-conversional methods (Vyazovkin, 1999). These methods make model-independent estimation of apparent activation energy at varying conversions possible, using thermogravimetric analysis at multiple heating rates (Vyazovkin, 1999). Some of the iso-conversional methods are presented below.

Flynn-Wall-Ozawa (FWO) method (Doyle approximation *p(x)*, Equation 11):

$$ln\beta = -1.0518\frac{E_a}{RT} + ln\frac{AE_a}{Rg(\alpha)} - 5.33 \quad (15)$$

Kissinger-Akahira-Sunose (KAS) method (CR approximation for *p(x)* for large *x*, Equation 12):

$$\ln\left(\frac{\beta}{T^2}\right) = \ln\left[\frac{AR}{E_a.g(\alpha)}\right] - \frac{E_a}{RT} \quad (16)$$

Starink method: (Starink approximation for *p(x)*, Equation 17).

$$p(x) = \frac{\exp(-1.0008x-0.312)}{x^{1.92}} \quad (17)$$

$$\ln\left(\frac{\beta}{T^{1.92}}\right) = -\frac{1.008\,E_a}{RT} + C \quad (18)$$

Kissinger method: $\ln\left(\frac{\beta}{T_p^2}\right) = \ln\left[\frac{AR}{E_a}\right] - \frac{E_a}{RT_p}$ (19)

T_p is the peak reaction rate temperature (K) for a given rate of heating.

Vyazovkin method: Vyazovkin (1997) employed a 4th-degree Senum and Yang approximation for *p(x)* (Equation 13) for better accuracy, and defined a function *Ω,* which when optimised would furnish the value of the apparent activation energy.

$$\Omega = \sum_{i=1}^{n} \sum_{j \neq i}^{n} \frac{I(i)}{I(j)} \frac{\beta(j)}{\beta(i)} \quad (20)$$

$I(i) = \frac{E_a}{R} p(x)$ represents the value of the function *I* at a given α at the heating rate β_i, while *n* denotes the number of rates of heating used. The non-linear procedure used in Vyazovkin method causes a smaller error in the activation energy (Vyazovkin, 1997).

Identification of the rate controlling step, g(α)

The rate controlling step may be identified by constructing a master-plot (Jankovic, 2008). g(α) values were calculated from different kinetic models: diffusion-controlled (D_n), phase boundary controlled (R_n), *n*-th order chemical reaction controlled (F_n), and Avrami Erofeev equation (nucleation and growth) controlled (A_n). Comparing it with the value at 50% conversion (Equation (9):

$$\theta_{model} = \frac{g(\alpha)}{g(\alpha=0.5)} = \frac{p(x)}{p(x)_{\alpha=0.5}} = \theta_{expt} \quad (21)$$

θ_{model} values were computed from the models at different values of α, while the corresponding θ_{expt} were calculated from the temperature integrals *p(x)* and $p(x)_{\alpha=0.5}$. An appropriate kinetic model was identified by the minimum mean RMS fractional error between the θ_{expt} *and* θ_{model} values.

Estimation of the thermodynamic properties of reaction

The thermodynamic properties of reaction were estimated from the following equations using the kinetic parameters *A* and E_a (Yuan *et al*., 2017).

$$A = \beta . E_a \exp\left(\frac{E_a}{RT_p}\right) / (RT_p^2) \quad (22)$$

$$\Delta H = E_a - R.T_\alpha \quad (23)$$

$$\Delta G = E_a + RT_p ln(\frac{k_B T_p}{hA}) \quad (24)$$

$$\Delta S = (\Delta H - \Delta G)/T_p \quad (25)$$

ΔS is the change in entropy, *ΔH is* the change in enthalpy, and *ΔG* is the change in Gibbs free energy. k_B and *h* are the Boltzmann constant the Planck's constant, respectively.

Some works were carried out on the thermal decomposition of CCH, and even fewer on ZHC. But different researchers presented divergent views on the mechanism of decomposition reactions for both hydroxide carbonates. This has been explained with greater clarity in this work, linking the thermogravimetric and FTIR results. Moreover, no comprehensive investigations have been published on the kinetic behaviour of these decomposition reactions, including the determination of the Arrhenius parameters with more recent kinetic analysis techniques and a comparative assessment, identifying the rate-controlling step, and estimation of changes in the thermodynamic properties of the reactions (*ΔH, ΔG* and *ΔS*). The present work was carried out to bridge this gap in the literature. The objectives of the present work were: (1) to determine the apparent activation energy and pre-exponential factor for thermal decomposition of CCH and ZHC using different nonisothermal model-free iso-conversional and model-fitting techniques, (2) to identify the rate-controlling regime for the reaction, (3) to estimate the changes in thermodynamic properties, and (4) to explain the reaction behaviour through kinetics, thermodynamics and FTIR analysis.

MATERIALS AND METHODS

Experimental

$CuCO_3.Cu(OH)_2$ (CCH) (analytical grade) was procured from SD Fine Chemicals, India, while $2ZnCO_3.3Zn(OH)_2$ (ZHC) (analytical grade), was obtained from Sigma Aldrich, India. Thermogravimetric analysis (TGA) was conducted in a thermogravimetric analyser (make: PerkinElmer, USA; model: STA 6000). 10 mg of sample was heated at the rate of 2, 5, 10, 15 and 20 $^oC.min^{-1}$ over the temperature range of 30-400 ^oC (for CCH) and 30-500 ^oC (for ZHC). TG and derivative thermogravimetric (DTG) plots were generated in the N_2-atmosphere at the flow rate of 20 $mL.min^{-1}$. All experiments were carried out thrice for repeatability, and the deviation was very low ($\pm$0.84%). The kinetic analysis computation was done using Microsoft Excel.

Vapours evolved from the decomposition of the sample from TGA were transported to an online FTIR analyser (make: PerkinElmer; Model: Spectrum II) coupled via hyphenation tube. The hyphenation tube and the FTIR analyser were kept at 300 and 250 ^oC, respectively, and the cell was kept heated to avoid any condensation of vapours. The FTIR spectrum of the volatiles evolved was continuously captured at an interval of 30 s.

RESULTS AND DISCUSSION

TG-DTG Curves

Figs. 1(a) and 1(b) show the TG and DTG plots for decomposition of CCH and ZHC samples at five heating rates; 2, 5, 10, 15 and 20 $^oC.min^{-1}$. ZHC was found to decompose at a higher temperature range than CCH. The reaction onset temperatures ($T_{0.05}$, at 5% conversion), peak-rate temperatures (T_p) and near-completion temperatures ($T_{0.95}$, at 95% conversion), characterising the decomposition, were observed to increase with the heating rate for both CCH and ZHC (Figs. 1(a) and 1(b), Table 1). For CCH, $T_{0.05}$ increased from 152.2 ^oC at 2 $^oC.min^{-1}$ to 219.9 ^oC at 20 $^oC.min^{-1}$, while $T_{0.95}$ increased from 219.5 ^oC (2 $^oC.min^{-1}$) to 273.1 ^oC (20 $^oC.min^{-1}$) (Table 1). Similarly, the DTG curves showed that peak-rate temperatures increased with the heating rate; from 208.67 ^oC (2 $^oC.min^{-1}$) to 249.6 ^oC (20 $^oC.min^{-1}$), and the peak-rate conversion decreased with the heating rate; from 0.617 (2 $^oC.min^{-1}$) to 0.484 (20 $^oC.min^{-1}$) (Fig. 1a). These primarily occurred due to the fact that a lower heating rate caused a higher sample residence time at the reaction temperature range, which caused greater decomposition at a given temperature. At a higher heating rate, the decomposition was delayed to a higher temperature due to the heat transfer resistance (Singh et al., 2018) with the thermal lag increasing with the rate of heating. This shifted both the TG and DTG curves to a higher temperature with the shift increasing with the rate of heating (Yuan, 2017).

Similar results were observed for ZHC where $T_{0.05}$ increased from 188.3 ^oC (2 $^oC.min^{-1}$) to 214.5 ^oC (20 $^oC.min^{-1}$) (Figs. 1(a) and 1(b), Table 1). Liu *et al*. (2004) and Kanari *et al*. (2004) observed the reaction to start at 220 ^oC and 200 ^oC respectively. $T_{0.95}$, increased from 335.5 ^oC (2 $^oC.min^{-1}$) to 358.7 ^oC (20 $^oC.min^{-1}$), while Henmi *et al*. (1986) observed the reaction to be completed at about 370 ^oC. Similarly, the peak-rate temperatures also increased with the heating rate; from 238.3 ^oC (2 $^oC.min^{-1}$) to 263.6 ^oC (20 $^oC.min^{-1}$). Liu *et al*. (2004) and Henmi *et al*. (1986) found the peak rate temperatures at 265.72 ^oC and 260 ^oC respectively at 20 $^oC.min^{-1}$. The conversions at the peak rate was not much influenced by the heating rate; 0.475 (2 $^oC.min^{-1}$) and 0.473 (20 $^oC.min^{-1}$) (Fig. 1b). The results showed that the impact of heating rate on $T_{0.05}$, $T_{0.95}$ and T_p, was less pronounced in ZHC than in CCH due to the difference in the rate of thermal diffusion inside the particles.

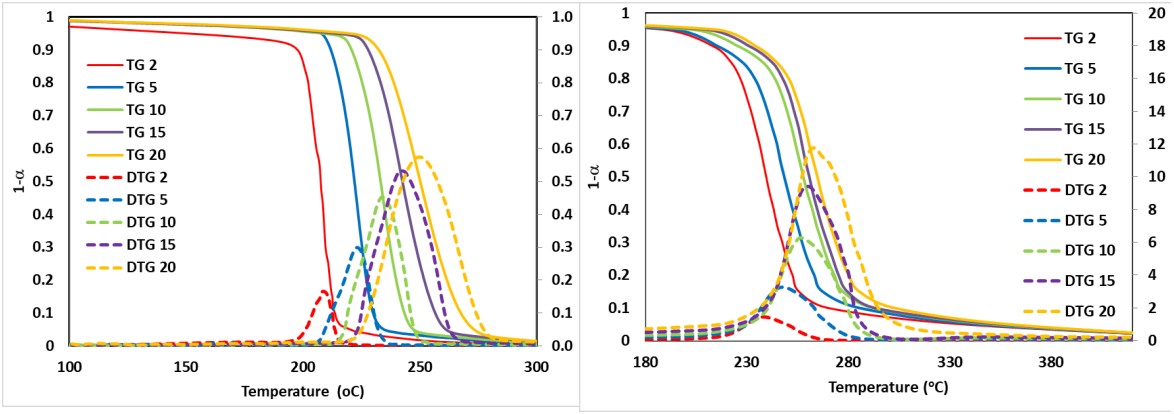

(a) **(b)**

Figure 1. Experimental TG and DTG curves at heating rates 2, 5, 10, 15, 20 ^{o}C.min^{-1}. (a) CCH, (b) ZHC

Table 1. Temperatures at 5% conversion, 95% conversion and peak reaction rate

Sample	**$CuCO_3.Cu(OH)_2$ (CCH)**					**$2ZnCO_3.3Zn(OH)_2$ (ZHC)**				
Heating Rate, ^{o}C.min^{-1}	2	5	10	15	20	2	5	10	15	20
$T_{0.05}$, ^{o}C	152.2	207.8	208.2	213.6	219.9	188.3	193.4	202.8	209.7	214.5
T_p, Peak rate Temperature, ^{o}C	208.7	223.2	233.8	242.5	249.6	238.3	247.6	256.7	259.8	263.6
$T_{0.95}$, ^{o}C	219.5	234.8	247.4	261.3	273.1	335.5	343.2	350.9	354.5	358.7

FTIR Analysis

At the outset, the solid samples CCH and ZHC were characterised by FTIR spectra (Fig. 2). The characteristic O-H stretching bond and ν_3 mode of carbonate bond was observed at around 3300 cm^{-1} (3200-3600 cm^{-1}) and 1380-1505 cm^{-1}, respectively, confirming their basic carbonate characteristics.

FTIR analysis of the gases produced from the degradation of CCH, heated at the rate of 10 ^{o}C.min^{-1} exhibited the first peak for the evolution of CO_2 in the range 2375-2290 cm^{-1} at 222 ^{o}C, (Fig. 3a). At this temperature, the mass loss was already about 5.6% (conversion 18.3%), while the stoichiometric mass loss of H_2O in CCH is 8.1% (29% conversion). Hence, substantial water loss had already taken place before decarboxylation started. While the Cu-OH bond is weaker than the Cu-OCO_2 bond (Brown, 1984), it is further weakened by the presence of oxy-salt anionic group like CO_3 (Ramamurthy and Secco, 1970). Dehydration and decarboxylation take place due to the rupture of these bonds. Frost et al. (2002) also reported that the dehydroxylation commenced before the onset of decarboxylation. At a later stage, the evolution of H_2O and CO_2 continued simultaneously due to concurrent dehydration and decarboxylation. The decarboxylation reaction was completed at about 272 ^{o}C (Fig. 3a), marking the end of reaction in the TG-DTG plots too (Fig. 1a).

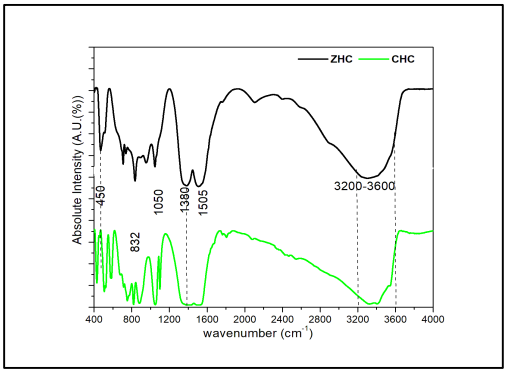

Figure 2. FTIR analysis of fresh CCH and ZHC samples

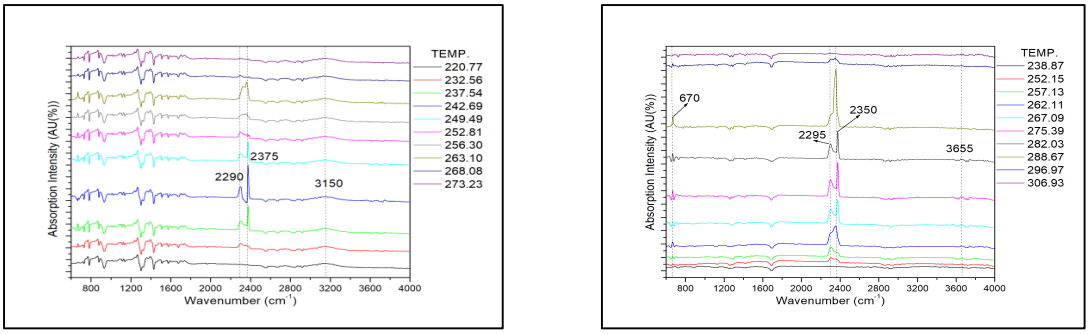

Figure 3. FTIR analysis of gases obtained from decomposition at different temperatures (^{o}C). (a) CCH, (b) ZHC

Similar FTIR analysis of the gases produced from ZHC decomposition at the heating rate of 10 ^{o}C.min^{-1} showed evolution of CO_2 starting at about 247 ^{o}C with peaks obtained in the range 2350-2295 cm^{-1} (Fig. 3b). Meanwhile, the mass loss of the sample was about 6.8% (24.8% conversion) where the stoichiometric mass loss of H_2O in ZHC is 9.84% (38% conversion). This showed that the dehydration had progressed significantly before the start of decarboxylation, following which the evolution of H_2O and CO_2 continued simultaneously. The decarboxylation reaction was completed at about 305^{o}C (Fig. 3b), which conformed to the TG-DTG data (Fig. 1b). Thus, the FTIR analysis of the evolved gases supported the fact that thermal decomposition of both CCH and ZHC started with the removal of water molecules, followed by simultaneous dehydration and decarboxylation reactions.

Kinetic Analysis of decomposition of CCH and ZHC

Estimation of apparent activation energy by model-free iso-conversional methods

Five model-free iso-conversional techniques were used for the kinetic study for comparison and confirmation. $ln\beta$, ln $(\frac{\beta}{T^2})$ and ln$(\frac{\beta}{T^{1.92}})$ were plotted against $1/T$ at fractional conversions of 0.10-0.90 (CCH) and 0.10-0.85 (ZHC) for FWO (Figs. 4a, 4c), KAS (Figs. 4b, 4d) and Starink methods, respectively (Equations 15, 16, 18). E_a at different conversions was obtained from the slope of the linear plots. Kissinger method was also employed to estimate E_a from the slope of the linear plot of ln $(\frac{\beta}{T_p^2})$ vs $1/T_p$ at different heating rates. E_a for the thermal decomposition of CCH and ZHC as determined by KAS, Starink, FWO, Kissinger and Vyazovkin methods are presented in Figs. 5a and 5b.

Activation energy is a measure of the minimum energy required to start the chemical reaction (Yuan, 2017). The E_a values estimated by KAS, Starink and Vyazovkin methods were observed to be almost identical at all conversion levels, while the values obtained from the FWO method were quite close too. Average values of E_a were estimated as 107.7, 104.9, 104.9, 111.2 and 105.2 kJ.mol^{-1} for CCH using KAS, Starink, FWO,

Kissinger and Vyazovkin methods, respectively. The same values for ZHC were found to be 192.8, 194.1, 194.3, 197.9 and 194.2 kJ.mol^{-1}. Very high regression coefficient, R^2 (0.991-0.995 for CCH and 0.985-0.986 for ZHC) for all methods showed that the experimental data agreed well with the models. The results showed that CCH was more reactive than ZHC, which had the higher apparent activation energy.

E_a for CCH decreased with conversion for all the methods - 125.6 to 89.9 kJ.mol^{-1} (FWO), 124.0 to 86.0 kJ.mol^{-1} (KAS), 123.9 to 85.9 kJ.mol^{-1} (Starink) and 124.2 to 86.3 kJ.mol^{-1} (Vyazovkin) with an increase in conversion from 0.10 to 0.90 (Fig. 5a). However, for ZHC, E_a (Fig. 5b) increased with conversion, from 186.3, 187.7, 187.9, 188.0 kJ.mol^{-1} to reach a peak of 199.9, 201.5, 201.7, 201.8 kJ.mol^{-1} at the conversion of 0.4, and then decreased for KAS, Starink, FWO, Vyazovkin methods respectively. As Vyazovkin method uses 4th-degree Senum and Yang approximation for $p(x)$ (Equation 13), which is more accurate than Doyle (Equation 11) and Coats and Redfern approximations (Equation 12) used in other model-free iso-conversional methods, along with non-linear optimisation, it generally results in a smaller error. However, in the present work, Vyazovkin, KAS and Starink methods produced nearly similar apparent activation energy values. The higher variation in E_a was observed in case of CCH than in ZHC. Multi-step reactions contribute to the global reaction mechanism to a different extent with varying conversion (Yuan, 2017). This suggests that the decomposition of CCH and ZHC is complex and cannot be characterised by a single-step reaction. The degree of complexity of the ZHC decomposition is, however, less than that of CCH, as reflected in the smaller variation in E_a. The sequence of dehydration and decarboxylation reactions (Figs. 3a and 3b) and the kinetics decide the global kinetics.

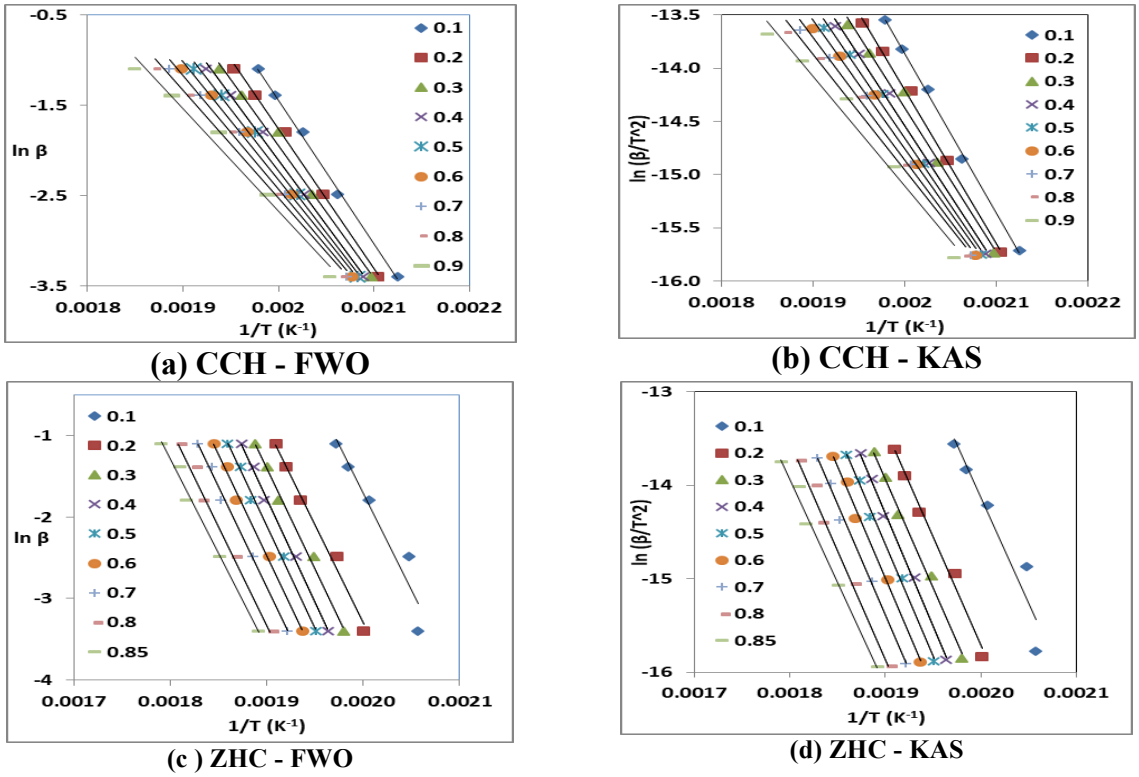

Figure 4. Estimation of apparent activation energy of decomposition of CCH and ZHC at different conversions using FWO and KAS methods

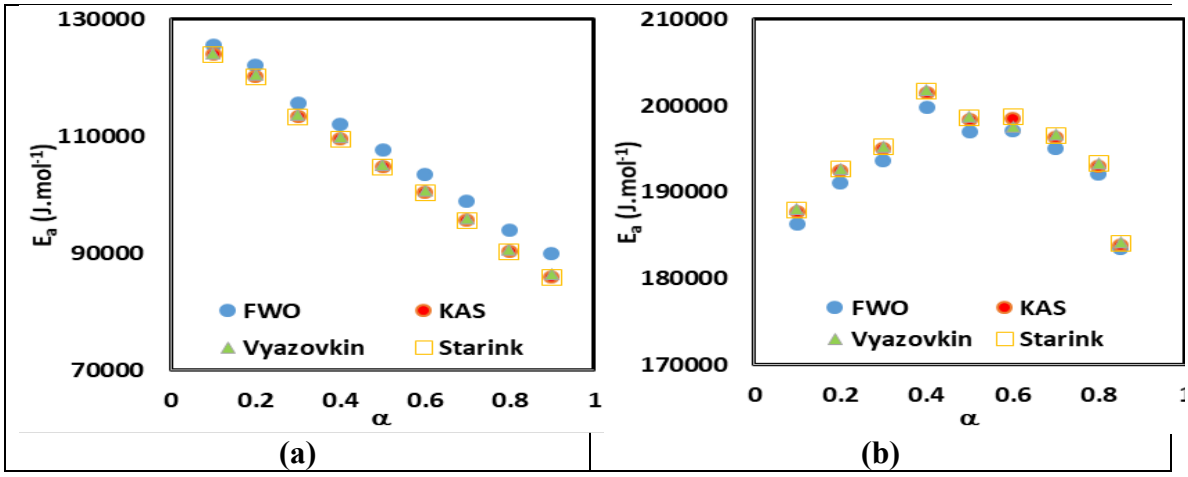

Figure 5. Variation of activation energy of decomposition with conversion (KAS, Starink FWO and Vyazovkin methods) (a) CCH, (b) ZHC

Identification of the rate-controlling regime

From the master-plot for CCH (Fig. 6a), random nucleation and growth was confirmed as the rate-controlling regime with the Avrami Erofeev equation exponent, *n*, optimised at 2.5 for the smallest error ($A_{2.5}$). A comparison between the model-predicted and experimental data showed that the agreement was good except at high conversions where, particularly at the higher heating rates, a lower value of Avrami Erofeev equation exponent, *n*, 1.5-2.0 fitted it better.

The master plot for ZHC (Fig. 6b) showed a good fit for the experimental points with $F_{1.75}$ over the entire range of conversion, and thus chemical reaction of order 1.75 was identified as the rate-controlling step. Similar results were obtained by KAS, Starink, FWO and Vyazovkin methods.

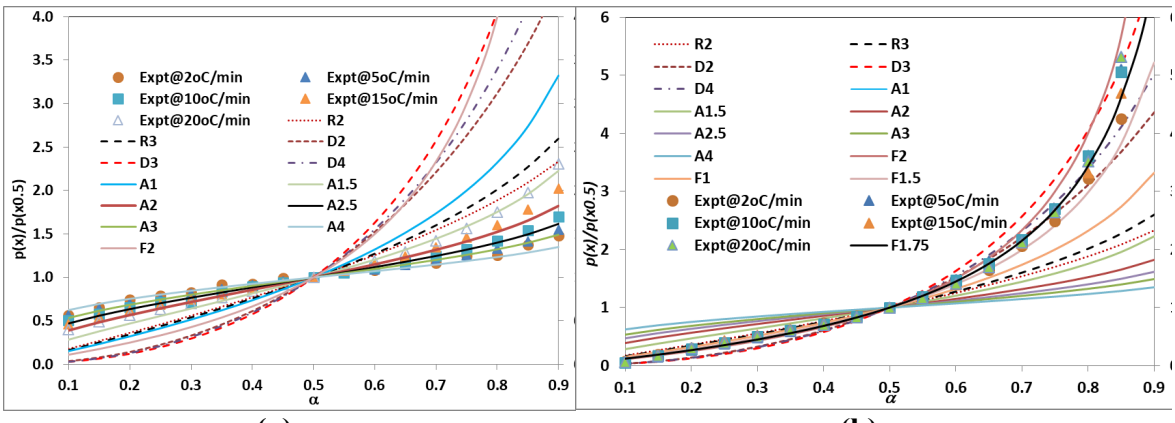

Figure 6. Identification of rate-controlling regime for the decomposition reaction using master-plot. Lines - *g(α)/g(0.5);* Points - *p(x)/p(x0.5)*. (a) CCH, (b) ZHC

Estimation of apparent activation energy by the model-fitting method

E_a was estimated from the slope of the linear plots of $\ln\left[\frac{g(\alpha)}{T^2}\right]$ vs *1/T* using Coats-Redfern (CR) method (Equation 14) with a mean R^2 value of 0.991 at five different heating rates. The average value of E_a for CCH (107.7 kJ.mol^{-1}) was found to agree well with the values obtained by the iso-conversional methods (104.9-111.2 kJ.mol^{-1}). However, E_a for ZHC (175.6 kJ.mol^{-1}) was found to be slightly higher (192.8-197.9 kJ.mol^{-1}).

Comparison of apparent activation energy and models with the published literature

The mean E_a for CCH decomposition estimated by six different methods (KAS, Starink, FWO, Kissinger, Vyazovkin and CR) (104.9-111.2 kJ.mol^{-1}) were in the range of values (79.5, 131.3, 133.8 kJ.mol^{-1}) obtained by Uzunov and Klissurski (1984), Koga *et al*. (1999, 2009). E_a for decomposition of ZHC estimated by the five iso-conversional methods (192.8-197.9 kJ.mol^{-1}) was in the same range (153, 241.86, 202 and 152.4 kJ.mol^{-1}) as determined by Kanari *et al*. (2004), Liu *et al*. (2004), Li *et al*. (2005) and Nobari *et al*. (2011). Avrami Erofeev equation ($A_{2.0,}$ $A_{1.8}$) was identified by Koga *et al*., 1999; Uzunov and Klissurski, 1984 as the kinetic model for CCH like the present work ($A_{2.5}$). Such investigations for ZHC are not available in the literature. The discrepancy in the apparent activation energy values for both CCH and ZHC, reported by various researchers, may have been caused by different sample sources, estimation of the temperature integral and experimental environments (Jankovic, 2008).

Estimation of the pre-exponential factor

The pre-exponential factor, A, of the reaction was estimated from Equation (22). The average values of A were found to be 9.49×10^8, 4.81×10^8, 4.71×10^8, 5.16×10^8, 2.25×10^9 and 9.04×10^8 s^{-1} for CCH and 2.58×10^{17}, 3.64×10^{17}, 3.80×10^{17}, 3.69×10^{17}. 4.92×10^{17}, 2.29×10^{15} s^{-1} for ZHC using KAS, Starink, FWO, Vyazovkin (Table 2), Kissinger and CR methods, respectively. The values obtained by all methods were found to be close except for the model-fitting CR method in case of ZHC due to a difference in E_a.

The pre-exponential factor, A, indicates the frequency of collision of the reactant molecules and is a useful indicator of the complexity and chemistry of a reaction (Singh *et al*. 2020). The empirically obtained pre-exponential factor for first-order reactions may be in the range 10^4-10^{18} s^{-1} (Turmanova *et al*., 2008). A small value of A ($<10^9$ s^{-1}) indicates a surface reaction, and if independent of the surface area, implies the formation of a tight or closed complex. A higher value of A ($>10^9$ s^{-1}) indicates a loose complex (Turmanova *et al*., 2008). The mean value of A for CCH was found to be ~ 10^9 s^{-1}, indicating a tight or closed complex being formed. However, the mean value of A for ZHC was found to be in the range of 10^{17} s^{-1}, suggesting the formation of a loose or simple activated complex. A larger value of A needs a higher rate of molecular collisions causing a slower degradation, requiring more reaction energy (Yuan *et al*., 2017).

The evaluated pre-exponential factor, though not impacted by the rate of heating, was influenced significantly by conversion for both CCH and ZHC. It decreased with conversion for CCH, while it increased to reach a peak and then decreased for ZHC in line with the change in E_a. This also suggested the decomposition reaction of both compounds to be of complex nature.

Estimation of the thermodynamic properties of the reactions

The thermodynamic properties of the reaction, ΔH, ΔG and ΔS, were calculated at different conversion and rates of heating using Equations (23-25) (Table 2). These properties too were not impacted much by the choice of iso-conversional methods. The variations in the mean ΔH, ΔG and ΔS for CCH were in the range 100.7-103.5 kJ.mol^{-1}, 146.8-146.9 kJ.mol^{-1}, -85.8 to -91.5 J.mol^{-1}.K^{-1} using KAS, Starink, FWO and Vyzovkin methods, respectively (Table 2). Similar variations for ZHC were 188.4-189.9 kJ.mol^{-1}, 151.1kJ.mol^{-1} and 71.0-73.8 J.mol^{-1}.K^{-1} (Table 2). The rate of heating had an even smaller effect on these thermodynamic properties. However, these were significantly impacted by the conversion. For CCH and ZHC, ΔH was 85.4-121.7 and 178.8-195.5 kJ.mol^{-1} and ΔS was -47.2 to -124.4 and 58.2-85.1 J.mol^{-1}.K^{-1} respectively over the range of conversion. However, the variation in ΔG was less; 144.4-149.4 and 150.1-152.5 kJ.mol^{-1} for CCH and ZHC, respectively. ΔH and ΔS showed similar trends with conversion as A and E_a, while ΔG showed a reverse trend. ΔH is the difference in enthalpy between the activated complex and the reactant (Yuan *et al*., 2017). Formation of the activation complex is favoured at a lower difference of E_a and ΔH (Singh *et al*., 2020). Low values of this difference in the present work; 3.9-4.5 and 4.0-4.6 kJ.mol^{-1} for CCH and ZHC respectively indicated that this small potential energy barrier would favour the reaction.

Gibbs free energy change, ΔG, denotes the rise in the total energy in the system to form the activated complex (Yuan *et al*., 2017). Positive ΔG values for both samples obtained in this study suggested that the decomposition reaction was not spontaneous (Table 2). A higher value of ΔG leads to lower reaction feasibility and greater energy requirement to sustain the reaction (Brown et al., 1984). The mean ΔG values for CCH and ZHC (146.8-146.9 and 151.1 kJ.mol^{-1} respectively) corroborated the present observations that CCH was more susceptible to decomposition than ZHC.

The change in activation entropy, ΔS, indicates the change in the degree of randomness or disorder in a reaction system. Negative average ΔS values for CCH (Table 2) showed that more ordered products were formed than the initial reactant through bond dissociation. Similar negative values of ΔS and positive values of ΔG and ΔH were observed by Tridane *et al*. (2015) in the decomposition of phosphates. However, ΔS was found to be positive for ZHC (Table 2), suggesting products to be less ordered than the reactants. A small ΔS value indicates that the reacting system has just passed through changes to bring the reaction systems near its own thermodynamic equilibrium, resulting in a low reactivity ((Turmanova *et al*., 2008).

Table 2. Mean pre-exponential factor and thermodynamic properties of reaction

	$CuCO_3.Cu(OH)_2$ (CCH)				**$2ZnCO_3.3Zn(OH)_2$ (ZHC)**			
Method	***A*, s^{-1}**	**ΔH, kJ.mol^{-1}**	**ΔG, kJ.mol^{-1}**	**ΔS, J.mol^{-1}.K^{-1}**	***A*, s^{-1}**	**ΔH, kJ.mol^{-1}**	**ΔG, kJ.mol^{-1}**	**ΔS, J.mol^{-1}.K^{-1}**
FWO	$9.49x10^{8}$	103.5	146.8	-85.8	$2.58x10^{17}$	188.4	151.1	71.0
KAS	$4.81x10^{8}$	100.8	146.9	-91.3	$3.64x10^{17}$	189.7	151.1	73.5
Starink	$4.71x10^{8}$	100.7	146.9	-91.5	$3.80x10^{17}$	189.9	151.1	73.8
Vyazovkin	$5.16x10^{8}$	101.1	146.9	-90.7	$3.69x10^{17}$	189.9	151.1	73.7

CONCLUSIONS

1. ZHC decomposed at a higher temperature range than CCH. Mean apparent activation energy and pre-exponential factor values for thermal decomposition of CCH and ZHC obtained by TGA using iso-conversional techniques like KAS, Starink, FWO, Vyazovkin method produced close results. The kinetic parameters obtained by the model-fitting CR method too matched well for CCH but deviated for ZHC.

2. The apparent activation energy decreased with a rise in conversion for CCH while it increased to reach a peak and then decreased for ZHC. This indicated that the reaction was not single-step. The degree of complexity of the ZHC decomposition reaction was, however, less than that of CCH, as reflected in the smaller variation in E_a.

3. Master-plots identified Avrami-Erofeev model ($A_{2.5}$) (random nucleation & growth model) as the rate-controlling regime for CCH and chemical reaction of order 1.75 ($F_{1.75}$) for ZHC. The models fitted the experimental TG data well for both samples except at very high conversions for CCH.

4. FTIR analysis of the gases produced from reactions showed that the decomposition of both CCH and ZHC started with dehydration, followed by simultaneous dehydration and decarboxylation reactions.

5. Thermodynamic properties ΔH, ΔG, and ΔS for CCH and ZHC decomposition were not influenced by the iso-conversional method and the rate of heating, but were impacted significantly by the conversion.

6. Positive changes in the thermodynamic properties, ΔH and ΔG, for both samples indicated that the endothermic decomposition process was not spontaneous. The activated complex formed through bond dissociation was more ordered than the initial reactant for CCH, while it was just the opposite for ZHC. Small differences between E_a and ΔH suggested both decomposition reactions to be favourable.

REFERENCES

Brown, I.W.M., Mackenzie, K.J.D. & Gainsford, G.J. 1984. Thermal decomposition of the basic copper carbonates malachite and azurite. Thermochimica Acta. **75**: 23-32. https://doi.org/10.1016/0040-6031(84)85003-0

Frost, R.L., Ding, Z. J., Kloprogge, T. & Martens, W.N. 2002. Thermal stability of azurite and malachite in relation to the formation of mediaeval glass and glazes. Thermochimica Acta. **390**: 133-144. https://doi.org/10.1016/S0040-6031(02)00127-2

Gupta, P., De, A. & Biswas. C. 2017. The Effect of Impurities on the Calcination Behaviour of $CaCO_3$ Nuggets. Journal of Engineering Research. **5**(1): 34-45. https://kuwaitjournals.org/jer/index.php/JER/article/view/1604

Henmi, H., Hirayama, T., Shanmugarajah, S., Mizutani, N. & Kato, M. 1986. Thermal decomposition of basic carbonates of copper, zinc and cobalt under high pressures. Thermochimica Acta. **106**: 263-271. https://doi.org/10.1016/0040-6031(86)85138-3

Jankovic, B. 2008. Kinetic analysis of the nonisothermal decomposition of potassium metabisulfite using the model-fitting and isoconversional (model-free) methods. Chemical Engineering Journal. **139**: 128-135. https://doi.org/10.1016/j.cej.2007.07.085

Kanari, N., Mishra, D., Gaballah, I. & Dupré, B. 2004. Thermal decomposition of zinc carbonate hydroxide. Thermochimica Acta. **410**: 93-100. https://doi.org/10.1016/S0040-6031(03)00396-4

Khawam, A. & Flanagan, D.R. 2006. Solid-State Kinetic Models: Basics and Mathematical Fundamentals. The Journal of Physical Chemistry B. **110**: 17315-17328. https://doi.org/10.1021/jp062746a

Koga, N., Criado, J.M. & Tanaka, H. 1999. Apparent kinetic behavior of the thermal decomposition of synthetic malachite. Thermochimica Acta. **340-341**: 387-394. https://doi.org/10.1023/A:1010172111319

Koga, N., Tatsuoka, T. & Tanaka, Y. 2009. Effect of atmosphericwater vapor on the kinetics of thermal decomposition of copper(II) carbonate hydroxide. Journal of Thermal Analysis and Calorimetry. **95**: 483-487. https://doi.org/10.1007/s10973-008-9271-0

Kurt, A. & Koca, M. 2016. Synthesis, characterization and thermal degradation kinetics of poly(3-acetylcoumarin-7-yl-methacrylate) and its organoclay nanocomposites. Journal of Engineering Research. **4**(4): 46-65. https://kuwaitjournals.org/jer//index.php/JER/article/view/1357

Li, Z., Shen, X., Feng, X., Wang, P. & Wu, Z. 2005. Non-isothermal kinetics studies on the thermal decomposition of zinc hydroxide carbonate. Thermochimica Acta. **438**: 102-106. http://dx.doi.org/10.1016/j.tca.2005.08.026

Liu, Y,. Zhao, J., Zhang, H., Zhu, Y. & Wang, Z. 2004. Thermal decomposition of basic zinc carbonate in nitrogen atmosphere. Thermochimica Acta. **414**: 121-123. http://dx.doi.org/10.1016%2Fj.tca.2003.12.004

Nobari, A.H., Pishahang, M. & Halali, M. 2011. Effect of CO2 Partial Pressure on the Thermal Decomposition Kinetics of Zinc Carbonate Hydroxide (TECHNICAL NOTE). International Journal of Engineering. **24**: 263-268. https://www.ije.ir/article_71922_50c55bbf3cb0784e5fa3290c3367c6df.pdf

Pourmortazavi, S.M., Kohsari, I. & Hajimirsadeghi, S.S. 2009. Electrosynthesis and thermal characterisation of basic copper carbonate nanoparticles. Central European Journal of Chemistry. **7**: 74-78. https://doi.org/10.2478/s11532-008-0094-4

Ramamurthy, P. & Secco, E.A. 1970. Studies on metal hydroxy compounds. XII. Thermal analyses, decomposition kinetics, and infrared spectra of copper basic oxysalts. Canadian Journal of Chemistry. **48**: 3510-3519. https://doi.org/10.1139/v70-587

Singh, R.K., Ruj, B., Jana, A., Mondal, S., Jana, B., Sadhukhan, A & Gupta, P. 2018. Pyrolysis of three different categories of automotive tyre wastes: Product yield analysis and characterisation. Journal of Analytical and Applied Pyrolysis. **135**: 379-389. https://doi.org/10.1016/J.JAAP.2018.08.011

Singh S., Chakraborty J.P. & Mondal, M.K. 2020. Intrinsic kinetics, thermodynamic parameters and reaction mechanism of non-isothermal degradation of torrefied Acacia nilotica using isoconversional methods. Fuel. **259**: 116263. https://doi.org/10.1016/j.fuel.2019.116263

Tridane, M. Fahim, I. Benmokhtar, S. & Belaaouad, S. 2015. Structural modifications from $NiNa_3P_3O_{10}.12H_2O$ to $NiNa_3P_3O_{10}$ new Triphosphate during dehydration process. Phosphorus Research Bulletin. **30**: 001-007. https://doi.org/10.3363/prb.30.1

Turmanova, S.C., Genieva, S.D., Dimitrova A.S. & Vlaev L.T. 2008. Non-isothermal degradation kinetics of filled with rise husk ash polypropene composites. Express Polymer Letter. **2**: 133–46. http://www.expresspolymlett.com/articles/EPL-0000524_article.pdf

Uzunov, I.M. & Klissurski, D.G. 1984. A thermogravimetric study of the decomposition of basic copper carbonate. Thermochimica Acta. **81**: 353-357.

Vyazovkin, S. 1997. Evaluation of activation energy of thermally stimulated solid-state reactions under arbitrary variation of temperature. Journal of Computational Chemistry. **18**: 393-402. https://doi.org/10.1002/(SICI)1096-987X(199702)18:3%3C393::AID-JCC9%3E3.0.CO;2-P

Vyazovkin, S. & Wight, C.A. 1999. Model-free and model-fitting approaches to kinetic analysis of isothermal and nonisothermal data. Thermochimica Acta. **340-341**: 53-68. https://doi.org/10.1016/S0040-6031(99)00253-1

Yuan X, He T., Cao H., & Yuan Q. 2017. Cattle manure pyrolysis process: Kinetic and thermodynamic analysis with isoconversional methods. Renewable Energy. **107**: 489–96. https://doi.org/10.1016/j.renene.2017.02.026